Active Temporal Multiplexing of Photons

Gabriel J. Mendoza, Raffaele Santagati, Jack Munns, Elizabeth Hemsley, Mateusz Piekarek, Enrique Martín-López, Graham D. Marshall, Damien Bonneau, Mark G. Thompson, and Jeremy L. O'Brien[1]

[1] *Centre for Quantum Photonics, H. H. Wills Physics Laboratory & Department of Electrical and Electronic Engineering, University of Bristol, Merchant Venturers Building, Woodland Road, Bristol, BS8 1UB, UK*

Quantum information science promises powerful new technologies and fundamental scientific discoveries [1]. Photonic qubits are appealing for their low noise properties—the cost is the non-deterministic nature of many processes, including photon generation and entanglement. Active multiplexing can increase the success probability of such processes above a required threshold, and spatial multiplexing of up to four heralded photon sources shows great promise [2–6]. The cost is a proliferation of hardware. Temporal multiplexing—repeated use of the same hardware components—has been proposed as an alternative [7–9] and is likely to be essential to greatly reduce resource complexity and system sizes. Requirements include the precise synchronization of a system of low-loss switches, delay lines, fast photon detectors, and feed-forward. Here we demonstrate multiplexing of 8 'bins'—four temporal and two spatial—from a heralded photon source. We show enhanced photon emission statistics, observing an increase in both the triggering and heralded photon rates. Despite its current limitations due to extrinsic sources of loss, this system points the way to harnessing temporal multiplexing in quantum technologies, from single-photon sources to large-scale computation.

Preparation and manipulation of exotic quantum states of light are at the heart of quantum information science and technology [1]. A central challenge is the non-deterministic nature of the generation of such states, which arises from nonlinear sources and negligible interaction between photons [10]. In particular, nonlinear sources of single photons have been the workhorse for proofs of principle to date because they generate photons in pairs, enabling heralding in highly pure spatio-temporal-spectral modes [11]. However, nonlinear sources have a theoretical maximum heralding efficiency of 25% [12], sufficient for some communication and sensing applications, but short of the best known threshold for computation [13]. As with other non-deterministic generation processes with heralded success signals, including fusion gates, for large-scale cluster states [13, 14], and ballistic entangled state generation [15–17], the success probabilities must be increased above relevant practical thresholds.

A promising approach is to actively multiplex (MUX) these processes by operating several copies in parallel, such that the probability of at least one succeeding is high, followed by a low-loss switching network to route a successful output into the downstream system [2, 14, 18]. Heralded photon sources, for example, require ∼8-16 copies for optimal operation [12, 19], and spatial multiplexing has been successfully implemented with up to four heralded photon sources [4–6]. Temporal multiplexing [7–9] (see Fig. 1) would enable repeated use of the same physical process, reducing resources, system size and indistinguishability requirements, at the cost of introducing delay lines and reducing the system clock rate. Temporal has been proposed for single-photon [7, 8] and entangled state generation [7, 9, 14, 20], as well as for photon memories [9] and boson sampling schemes [21].

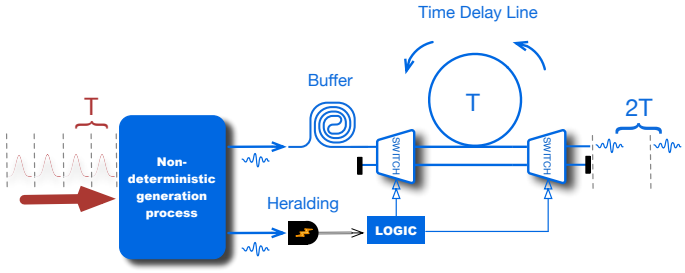

Figure 1: **Illustration of the principle of temporal multiplexing.** A non-deterministic generation process is repeated in time with period T; on heralded success, an active optical switching network and delay lines offset photons into output time bins spaced by an integer multiple of the input period and in sync with the system clock cycle. With a sufficiently low-loss switching network, the generation probability per clock cycle is increased.

Here, we demonstrate active temporal multiplexing and use it to improve the success probability of a heralded single-photon source. By combining temporal with spatial multiplexing using a double-passed heralded source, only a single physical source was used to enable hybrid spatial-temporal multiplexing of eight effective source repetitions. We show active time multiplexing of a source of periodic photons (previous demonstrations have shown passive temporal multiplexing [22] and active storage, but not multiplexing, of photons from non-periodic sources using cavities [23, 24]) to increase the heralded photon rate by up to 59% compared to our most efficient non-multiplexed source.

Our experimental setup (shown in Fig. 2 and further explained in Supplementary Material I) uses a bulk periodically-poled lithium niobate (PPLN) down-

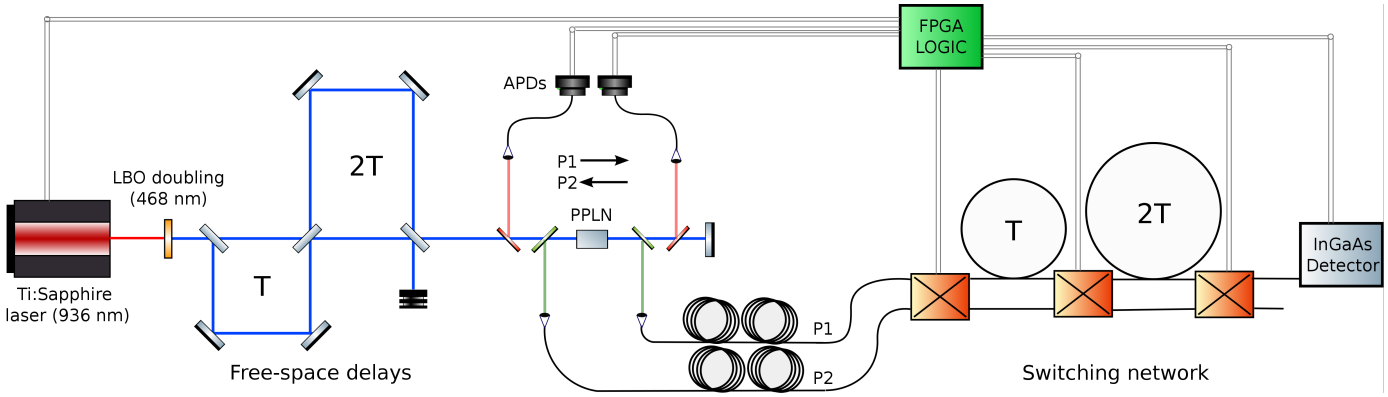

Figure 2: **Experimental setup.** Pulses from a femtosecond laser are upconverted using an LBO crystal, split into four copies using free-space delay lines, and passed twice through a PPLN crystal for down-conversion. Following separation of the photon pairs and pump using filtering, the heralding signals are analyzed by an oversampling FPGA while the signal photons are stored in long fiber delays. The FPGA configures the switching network to deliver the generated signal photons into a single spatial and temporal mode. P1 and P2 indicate Pass 1 and Pass 2.

conversion crystal phase-matched to produce idler photons at 671 nm and signal photons at 1547 nm from a pump laser at 468 nm. These wavelengths enable high-efficiency detection of the idler photon using silicon avalanche photodiodes (APDs) and low-loss transmission of the signal photon through switches and fiber delay lines.

Each pulse from a pump laser with a 80 MHz repetition rate (12.5 ns pulse spacing) is frequency doubled and split into four pulses spaced by ∼3 ns using a series of free-space delay lines constructed from beam-splitters and mirrors. The four pulses then pass through the PPLN crystal and undergo collinear down-conversion, probabilistically creating photon pairs in four time bins in the first spatial mode (referred to as Pass 1); a return pass of the pump through the crystal, obtained by recycling the residual pump reflected from a mirror, creates four additional time bins in a separate spatial mode (Pass 2). The setup was designed to keep the pump beam profiles for the four delays in both Pass 1 and Pass 2 as identical as possible. The spectra of the signal photons from all eight effective sources were shown to have a high degree of similarity (see Supplementary material II) and an in-line polarizer was used to verify their identical polarization.

The active optical switching network is composed of low-loss fiber switches (∼1 dB loss per switch, 500 kHz maximum operation frequency) and fiber delay lines matched to the free-space delay lines (see Fig. 2) in a binary division configuration [7, 8]. Detection signal time bins are discriminated using a fast oversampling Field Programmable Gate Array (FPGA), which then configures the switches for feed-forward multiplexing of the eight time and spatial modes. To avoid driving the switches faster than their maximum operation frequency, an asynchronous deadtime of 2 μs was programmed into the FPGA to limit the rate of detected heralding signals. During heralding detection, feed-forward processing, and switch configuration, the signal photons are stored in long delay lines of telecom fiber. Signal photons are detected using an InGaAs detector, gated from the idler photon detection events.

Photon counting statistics were collected for the eight non-multiplexed sources and the multiplexed source. Triggering (idler singles) rates and heralded signal photon (coincidence) rates (see Methods) are shown in Fig. 3 (accidental rates are shown in Supplementary material III). The data was taken at different reference powers, defined as the average power of the pump laser in front of the PPLN crystal used to generate the photons. A fraction of the reference power corresponds to the power used to pump each of the non-multiplexed sources individually (∼25% for Pass 1 delays and, due to power loss, ∼12.5% for Pass 2 delays). The triggering rates were affected by saturation loss caused by the limited switch operation frequency (500 kHz), which necessitated a large asynchronous deadtime to be programmed into the FPGA to avoid triggering detection faster than this rate. With the overall clock rate of the source set by the 80 MHz repetition rate of the pump laser, the multiplexed source suffered from greater saturation effects at high powers due to this deadtime than the less-deterministic heralded source, as can be seen in the sharp bending of the data away from a linear trend as the reference power is increased in Fig. 3a.

The data were found to be in excellent agreement with our model of the heralded and multiplexed sources (see Supplementary material IV), as shown in Fig. 3. According to the fit, the 4× time multiplexed source (composed of all Pass 1 delays) showed an increase of up to 175% in the triggering rate compared to the most efficient non-multiplexed source (Pass 1, Delay 3) and the 8× time and space multiplexed source (composed of both Passes, all

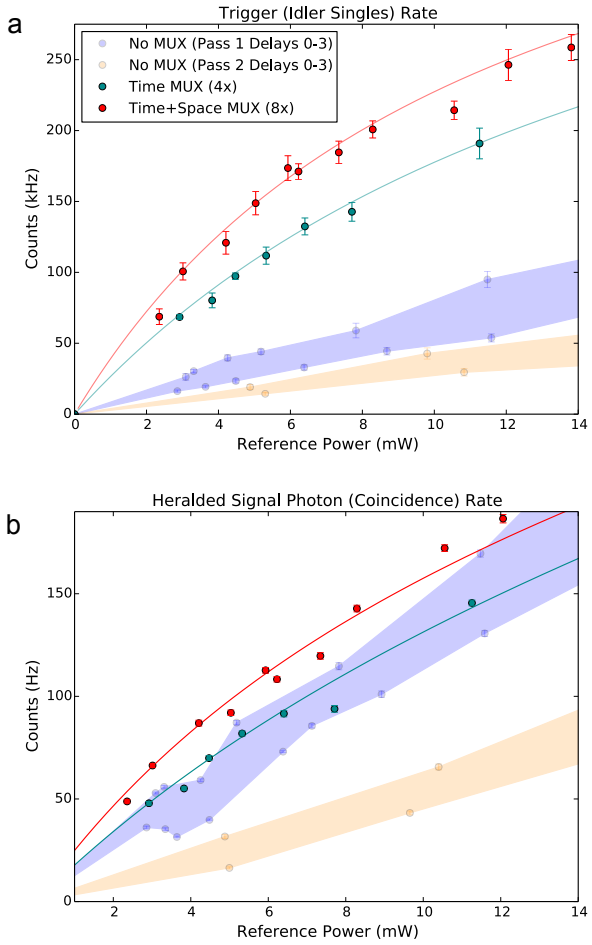

Figure 3: **Photon statistics from multiplexed and non-multiplexed sources. a,** Triggering (idler singles) and **b,** and heralded signal photon (coincidence) rates vs. reference laser pump power for the 8× multiplexed, 4× multiplexed, and non-multiplexed sources. For clarity of presentation, data points from the non-multiplexed sources are shown as linearly interpolated region plots encompassing the range of data: blue (Pass 1, Delays 0-3) and orange (Pass 2, Delays 0-3). Theory lines for the multiplexed sources are calculated from measured heralded source parameters, measured switch loss, and extrinsic loss effects.

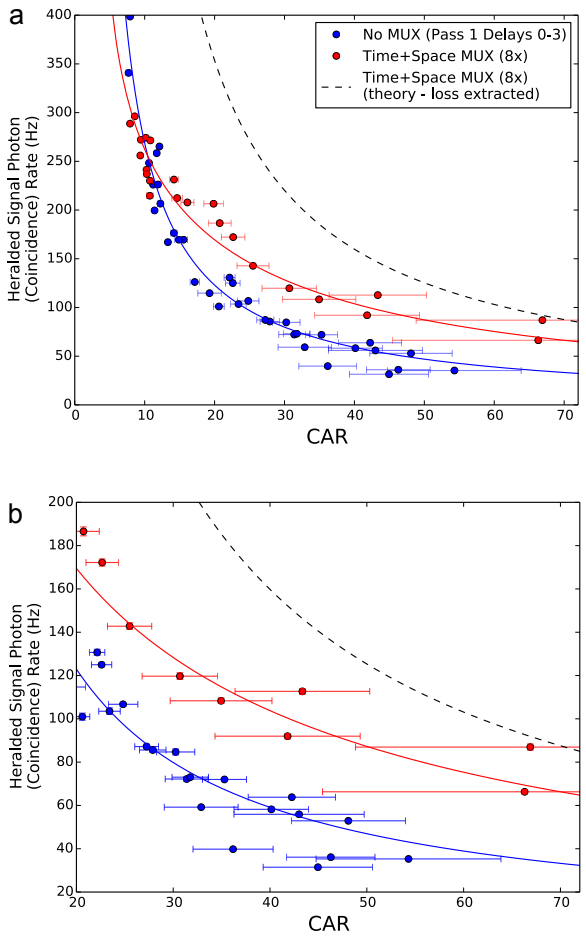

Figure 4: **Heralded signal photon (coincidence) rate vs. CAR for multiplexed and non-multiplexed sources. a,** Shows the full data set, and **b,** shows detail at low powers, where saturation effects due to electronics are small. Red points are for the 8× multiplexed source, and blue points are for the non-multiplexed sources (Pass 1). Solid lines are based on a theory fit using measured parameters. Dashed line shows a correction for extrinsic sources of loss based on the theory model.

delays) showed up to a 290% increase (see Fig. 3a). At low reference powers (2.5-10.5 mW), coincidence rates for the 4× multiplexed source were comparable to the non-multiplexed source with the highest coincidence rates, while the 8× multiplexed source showed a higher coincidence rate than any individual non-multiplexed source (see Fig. 3b). At high powers, the rates of coincidences for the multiplexed sources were suppressed due to the saturation of triggering events, as predicted by our model (Supplementary material IV).

The coincidence to accidental ratio (CAR) serves as a measure of noise due to single-photon emission and multi-photon contamination probabilities; this measure of noise cannot be inferred from coincidence rates alone. The heralded photon rate for fixed CAR, therefore, is the key measure of performance for our multiplexed source, and is plotted in Fig. 4 (data from the 4× multiplexed source is shown in Supplementary material III). For a fixed CAR, in the regime where saturation effects are small, the 4× multiplexed source did not show a significant increase in the heralded photon rate, and was limited mainly by the loss of the switching network (∼4 dB loss for each path). However, the 8× multiplexed source exhibited an increased heralded photon rate between 33-59% over the best non-multiplexed source and between 47-76% over the mean from the non-multiplexed sources (Pass 1 only), demonstrating a direct improve-

ment (Fig. 4b). In our model we corrected for the effects of extrinsic loss on the rate of heralded photon production (dashed line Fig. 4a, see Methods and Supplementary material IV), indicating a potential improvement of ∼114% for a wide range of CAR values compared to the non-multiplexed sources (also with extrinsic loss removed). This enhancement can be mapped to a comparable increase in the single-photon emission probability for a fixed multi-photon emission probability (see Supplementary material V).

Although our multiplexed photon source was limited by the maximum operation frequency of the switches, we note that even low rate, high efficiency sources will likely find applications in the near term, due to the improved generation probability of the sources per clock cycle. Ultimately, the development of a lower-loss, high-speed optical switch will enable a near-deterministic source with the highest single-photon emission rates. Such a high rate source will enable demonstration of quantum interference between different multiplexed sources, verifying photon purity. Improved multiplexing components and sources will further enable the temporal multiplexing of more complex generation processes, such as fusion gates or ballistic entangled state generation, where phase stability will be essential.

Temporal multiplexing techniques will almost certainly be required in future large-scale quantum circuits in order to substantially reduce resource requirements. Furthermore, hybrid temporal and spatial multiplexing techniques will be important in order to optimize tradeoffs between spatial footprint and system clock rate. Integrated photonic components, including sources (e.g. [25]), switches (e.g. [26]), filters (e.g. [27]), delay lines (e.g. [28]), and detectors (e.g. [29]), are under development. Scaling down our set-up to a fully integrated photonic chip with low-loss components will enable a temporal multiplexing template capable of realizing new classes of quantum information experiments and technology.

Acknowledgements

We thank Xiao Ai, Daryl Beggs, Allison Rubenok, Gary Sinclair, Ivo Straka, Jianwei Wang, Andrew Young, and Xiou-Qi Zhou for useful discussions and assistance. This work was supported by EPSRC, ERC, PICQUE, BBOI, US Army Research Office (ARO) Grant No. W911NF-14-1-0133, U.S. Air Force Office of Scientific Research (AFOSR). J.L.O'B. acknowledges a Royal Society Wolfson Merit Award and a Royal Academy of Engineering Chair in Emerging Technologies. G.D.M. acknowledges the FP7 Marie Curie International Incoming Fellowship scheme.

METHODS

A mode-locked, Ti:Sapphire laser (Tsunami, Spectra Physics) produced ∼150 femtosecond pulses at 936 nm; a LBO crystal (Newlight) was used to frequency convert to 468 nm. The pulsed laser was locked-to-clock, producing a reference pulse input to the FPGA. To enable low-loss, near 50-50 splitting of the pulsed pump beam, laser line non-polarizing beamsplitters (Newport) were used in the free space delays. The PPLN crystal (Covesion) was 3 mm long and phase-matched at 110° C using an oven and temperature controller. Dichroic mirrors (Semrock) were used to separate the signal and idler photons from the pump, and Pellin-Broca prisms were used for further spatial filtering. A bandpass filter center at 671 nm (Semrock) was used on the idler arms for each pass for further filtering. Pump leakage and dark counts were found to be negligible on the heralding (idler) arms. Switches (Agiltron, ∼1 dB loss per switch, 500 kHz repetition rate) were based on an electro-optic material. Standard telecom fiber was used for the variable delay loops and long delay lines (∼700 m, ∼90% transmission). To enable reliable comparison between multiplexed and non-multiplexed source measurements, a MEMS switch with nearly balanced loss was used to route the photons into or around the multiplexing switch network.

Coincidence counts, joint detection between idler and signal photons from paired generation events, were collected using gated detection of the signal photon from idler detection events. Accidental counts, joint detection between idler and gated signal photons from unpaired generation events, were then collected by shifting the temporal delay of the gating window by a multiple of the clock cycle. Pump leakage in the signal arms was found to be negligible at the measured powers. Dark counts detected by the InGaAs detectors in gated mode were measured by blocking the signal arm path; these counts were then subtracted from the count totals. The gate width used was 1.8 ns.

Extrinsic Sources of Loss: Extrinsic source of loss in the setup include: 1) Loss due to measurement apparatus. A small amount of extra loss (4%) on the multiplexed source was due to asymmetric loss of the MEMS switch used to switch between multiplexing and non-multiplexing channels for measurement. 2) Loss due to the deadtime of available electronic amplifiers. The two electronic amplifiers used to amplify the signal from the APD and into the FPGA have deadtimes of ~ 0.1 μs, resulting in missed pulses from the APD. In principle, much faster amplifiers with negligible deadtimes can be used to eliminate this source of loss. 3) Loss due to the limited switch repetition rate (500 kHz). An asynchronous deadtime of 2 μs was programmed into the FPGA to avoid driving the switches faster than their 500 kHz repetition rate. The switch repetition rate is set by the switch driver board; the switches themselves have a faster intrinsic rise and fall time of 300 ns ($\sim$ 3 MHz).

[1] J. W. Pan, Z.B. Chen, C.Y Lu, H. Weinfurter, A. Zeilinger, and M. Żukowski. Multiphoton entanglement and interferometry. *Rev. Mod. Phys.*, 84:777-838, 2012.

[2] A. L. Migdall, D. Branning, and S. Castelletto. Tailoring single-photon and multiphoton probabilities of a single-photon on-demand source.. *Phys. Rev. A*, 66(5):053805, 2002.

[3] J. H. Shapiro and F. N. Wong. On-demand single-photon generation using a modular array of parametric downcon- verters with electro-optic polarization controls. *Opt. Lett.*, 32(18):2698-2700, 2007.

[4] X. Ma, S. Zotter, J. Kofler, T. Jennewein, and A. Zeilinger. Experimental genera- tion of single photons via active multiplexing.. *Phys. Rev. A*, 83(4):043814, 2011.

[5] M. J. Collins, C. Xiong, I.H. Rey, T. D. Vo, J. He, S. Shahnia, C. Reardon, T. F. Krauss, M. J. Steel, A. S. Clark, and B. J. Eggleton. Integrated spatial multiplexing of heralded single-photon sources. *Nat. Comm.*, (20):10.1038, 2013.

[6] T. Meany, L. A. Ngah, M. J. Collins, A. S. Clark, R. .J Williams, B. J. Eggleton, M. J. Steel, M. J. Withford, O. Alibart, and S. Tanzilli. Hybrid photonic circuit for multiplexed heralded single photons. *Laser and Photonics Reviews*, 8(3):L42-L46, 2014.

[7] J. Mower and D. Englund. Efficient generation of single and entangled photons on a silicon photonic inte- grated chip.. *Phys. Rev. A*, 84(5):052326, 2011.

[8] C. T. Schmiegelow and M. A. Larotonda. Multiplexing photons with a binary division strategy. *Appl. Phys. B*, 116(2):447-454, 2013.

[9] T. B. Pittman, M.J. Fitch, B.C. Jacobs, and J.D. Franson. Periodic single-photon source and quantum memory. *Proc. SPIE*, 5161, 2004.

[10] E. Knill, R. Laflamme, and G.J. Milburn. A scheme for efficient quantum computation with linear optics. *Nat.*, 409(6816):46-52, 2001.

[11] M. D. Eisaman, J. Fan, A. Migdall, and S. V. Polyakov. Single-photon sources and detectors.. *Review of Scientific Instruments*, 82(7):071101, 2011.

[12] A. Christ and C. Silberhorn. Limits on the deterministic creation of pure single-photon states using parametric down-conversion. *Phys. Rev. A*, 85(2):023829, 2012.

[13] D. E. Browne and T. Rudolph. Resource-efficient linear optical quantum computation. *Phys. Rev. Lett.*, 95:010501, 2005.

[14] M. G. Segovia, P. Shadbolt, D. E. Browne, and T. Rudolph. From three-photon GHZ states to universal ballistic quantum computation. *ArXiv Preprint*, 2014.

[15] Q. Zhang, X. H. Bao, C.Y. Lu, X. Q. Zhou, T. Yang, T. Rudolph, and J.W. Pan. Demonstration of a scheme for the generation of event- ready entangled photon pairs from a single-photon source. *Phys. Rev. A*, 77:062316, 2008.

[16] M. Varnava, D. Browne, and T. Rudolph. How Good Must Single Photon Sources and Detectors Be for Efficient Linear Optical Quantum Computation? *Phys. Rev. Lett.*, 100(6):060502, 2008.

[17] H. Cable and J. Dowling. Efficient Generation of Large Number-Path Entanglement Using Only Linear Optics and Feed-Forward. *Phys. Rev. Lett.*, 99(16):163604, 2007.

[18] T. Jennewein, M. Barbieri, and A. G. White. Single-photon device requirements for operating linear optics quantum computing outside the post- selection basis. *Journ. of Mod. Opt.* , 58(3-4):276287, 2011.

[19] D. Bonneau, G. J. Mendoza, J. L. O'Brien, and M. G. Thompson. Effect of Loss on Multiplexed Single-Photon Sources. *ArXiv Preprint*, 2014.

[20] K.T. McCusker and P.G. Kwiat. Efficient optical quantum state engineering. *Phys. Rev. Lett.*, 103:163602, 2009.

[21] P. P. Rohde. Simple scheme for universal linear-optics quantum computing with constant experimental complexity using fiber loops. *Phys. Rev. A*, 91:012306, 2015.

[22] M. A. Broome, M. P. Almeida, A. Fedrizzi, and A. G. White. Reducing multi-photon rates in pulsed down-conversion by temporal multiplexing. *Optics Express*, 19(23):2269822708, 2011.

[23] T. B. Pittman, B. C. Jacobs, and J. D. Franson. Single photons on pseudodemand from stored parametric down-conversion. *Phys. Rev. A*, 66:042303, 2002.

[24] J. Yoshikawa, K. Makino, S. Kurata, P. van Loock, and A. Furusawa. Creation, storage, and on-demand release of optical quantum states with a negative wigner function. *Phys. Rev. X*, 3:041028, 2013.

[25] J. Silverstone, D. Bonneau, K. Ohira, N. Suzuki, H. Yoshida, N. Iizuka, M. Ezaki, C.M. Natarajan, M.G. Tanner, R.H. Hadfield, V. Zwiller, G.D. Marshall, J.G. Rarity, J.L. OâĂŹBrien, and M.G. Thompson. On-chip quantum interference between silicon photon-pair sources. *Nat. Phot.*, 8(2):104-108, 2014.

[26] C. Lacava, M. J. Strain, P. Minzioni, I. Cristiani, and M. Sorel. Integrated nonlinear Mach Zehnder for 40 Gbit/s all-optical switching. *Opt. Expr.*, 21(18):21587âĂŞ21595, 2013.

[27] S. H. Jeong, D. Shimura, T. Simoyama, M. Seki, N. Yokoyama, M. Ohtsuka, K. Koshino, T. Horikawa, Y. Tanaka, and K. Morito. Low-loss, flat-topped and spectrally uniform silicon-nanowire-based 5th-order CROW fabricated by ArF-immersion lithography process on a 300-mm SOI wafer. *Opt. Expr.*, 21(25):30163âĂŞ30174, 2013.

[28] H. Lee, T. Chen, J. Li, O. Painter, and K. J Vahala. Ultra-low-loss optical delay line on a silicon chip.. *Nat. Comm.*, 3:867, 2012.

[29] F. Marsili, V.B. Verma, J.A. Stern, S. Harrington, A.E. Lita, T. Gerrits, I. Vayshenker, B. Baek, M. D. Shaw, R.P. Mirin, and S.W. Nam. Detecting single infrared photons with 93% system efficiency. *Nat. Phot.*, 7(3):210-214, 2013.

[30] W. Grice, A. U'Ren, and I. Walmsley. Eliminating frequency and space-time correlations in multiphoton states. *Phys. Rev. A*, 64(6):063815, 2001.

[31] C. Gerry and P. Knight. Introductory Quantum Optics. *Cambridge University Press*, 2004.

[32] G. F. Knoll. Radiation Detection and Measurement. *2nd ed. Wiley*, New York 1989.

Supplementary Material: Active Temporal Multiplexing of Photons

I. PRINCIPLE OF OPERATION

A schematic of a heralded single-photon source (HSPS) is shown in Fig. S1a). A pulsed laser pumps a nonlinear material, spontaneously generating photon pairs, called signal and idler photons, in a fixed time bin. Assuming spectral disentanglement [S30], the state after the crystal is given by an infinite superposition of Fock state pairs [S31]:

$$|\psi\rangle = \sqrt{1-|\xi|^2}\left(|0\rangle_i\,|0\rangle_s + \sum_{n=1}^{\infty}\xi^n\,|n\rangle_i\,|n\rangle_s\right), \tag{S1}$$

where i and s are the idler and signal modes and ξ is the squeezing parameter determined by the pump power and the strength of the nonlinearity. Multi-photon pairs generally result in detrimental effects in quantum circuits, necessitating low squeezing parameters so that the single-pair term in (1) dominates.

Filters are used to separate the signal and idler photon and the pump, and a single-photon detector placed on

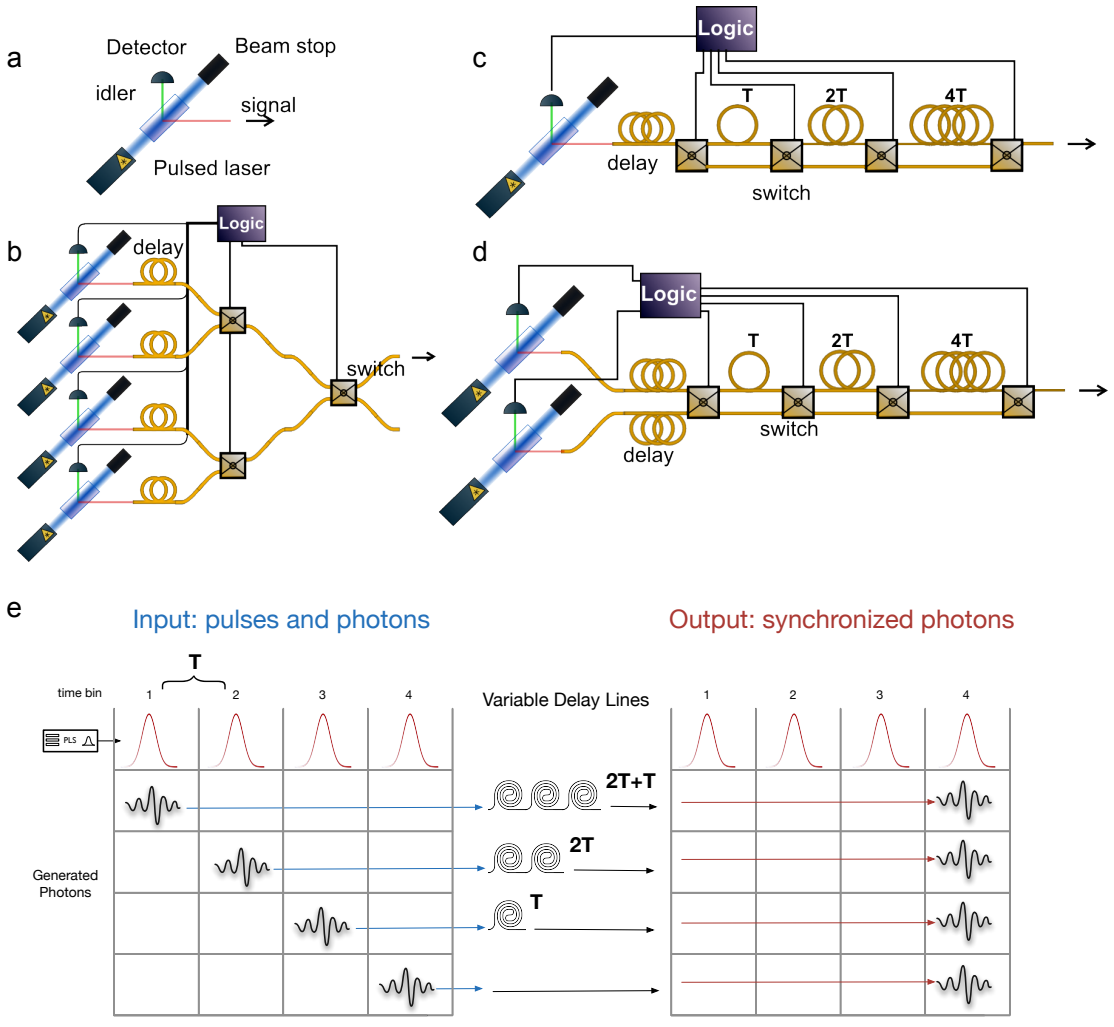

Figure S1: **Illustration of multiplexed single-photon sources and principle of operation a,** Heralded single-photon source. **b,** Spatially multiplexed single-photon source. **c,** Time multiplexed single-photon source. **d,** Time and space multiplexed single-photon source (See text for details). **e,** Principle of operation with four time bins. Photons generated probabilistically from laser pulses in four time bins are offset into a single time bin using variable delay lines and an active switching network.

the idler arm is used to herald the presence of the signal photon. Under ideal conditions and with number-resolving detectors, the theoretical maximum single-photon emission probability of a HSPS is limited to 25% [S12], due to the presence of multi-photon pair terms in equation (1). While this single-photon emission probability is sufficient for small-scale quantum optics experiments, heralded sources by themselves are not sufficient for scalable quantum technology [S19].

A spatial multiplexing technique (Fig S1b), which uses an array of HSPSs, delay lines, and electronics for feed-forward, can be used to boost the single-photon emission probability while suppressing multi-photon contamination [S2, S3]. With high probability, at least one of the HSPSs will emit a single-photon pair; detection of the idler photon is again used to herald the emission of the signal photon. Fast feed-forward and an active switching network are then used to route the heralded photon into a single mode output. The switching network is composed of 2×2 switches and has a depth of $\log(N)$, where N is the number of HSPSs. If every source in the multiplexed source is assumed to be identical, the probability of single-photon emission is

$$p_{single}^{MUX} = \left(1 - (1 - p_{trig})^N\right) p_{single}, \tag{S2}$$

where p_{trig} is the probability that each HSPS triggers and p_{single} is the triggered single-photon emission probability of each HSPS after passing through the switching network [S19]. The probability of multi-photon contamination, p_{multi}^{MUX}, remains approximately the same as in a non-multiplexed heralded source. With ideal operation and assuming a lossless switching network, 17 heralded sources enable a source with >99% single-photon emission probability [S12], and assuming realistically small losses, ∼8-16 heralded sources enable a near-deterministic source for large-scale applications [S19].

Besides multiplexing using many repetitions of the heralded source in space, a complementary approach is temporal (time) multiplexing of heralded single-photon sources [S7, S8]. In this scheme, a single heralded source is used with a series of switches and time delay loops (Fig. S1c). The heralded source is pumped N times with laser pulses spaced by time T, and delay lines (with lengths of integer multiples of T, which we will call variable delay lines) offset probabilistically generated photons into a single spatial-temporal mode (Fig. S1e). The switching network is capable of uniquely routing a photon generated in any of the input bins to a fixed output bin; if multiple photons are heralded in several input bins, the extra photons are automatically removed into adjacent bins. Time multiplexing with N time bins requires a depth of log(N) switches, and besides the loss of the variable delay lines, produces the same effects as spatial multiplexing while requiring only a single heralding source (which includes nonlinear material, detectors, and filters) and fewer switches.

Finally, in this work we implemented a hybrid scheme using two spatially multiplexed sources fed into a time multiplexing set-up, doubling the number of effective source repetitions (Fig. S1d). By using a return pass in the opposite direction through the same nonlinear crystal, hybrid time and spatial multiplexing can be implemented with only a single nonlinear source. This scheme enables an additional enhancement to the single-photon emission probability without an additional loss penalty, since the same depth of switches as the time multiplexing scheme is used.

II. SPECTRAL DATA AND SOURCE DETAILS

Although Pass 2 should ideally be identical in operation to Pass 1, it differs from Pass 1 in two aspects. First, the laser pump power passing through the down-conversion crystal has been reduced by ∼50% compared to the first pass, due to loss from the crystal without anti-reflection coating (∼15% pump loss per facet) and additional loss from dichroic mirrors used for filtering. Second, Pass 2 is affected by unwanted "back-reflected" photons from the Pass 1, again due to a lack of anti-reflection coating and the cut of the crystal. These back-reflected photons result in false heralding events, degrading the quality of the multiplexed source. By optimizing the position of the crystal, the back-reflected photon contamination in Pass 2 can be minimized (∼20% of the total counts on the idler arm and ∼8% of the total counts on signal arm). These features were taken into account during the modeling and analysis of results (Supplementary material IV). We estimate that <5% of heralding events at all powers tested in the 8× multiplexed source can be attributed to "false" heralding events caused by back-reflected photons. Despite the reduced power and contamination from back-reflected photons affecting Pass 2, the spectral properties of the signal and idler photons from all eight effective sources are shown to have a high degree of similarity (Fig. S2) and an in-line polarizer verified their identical polarizations.

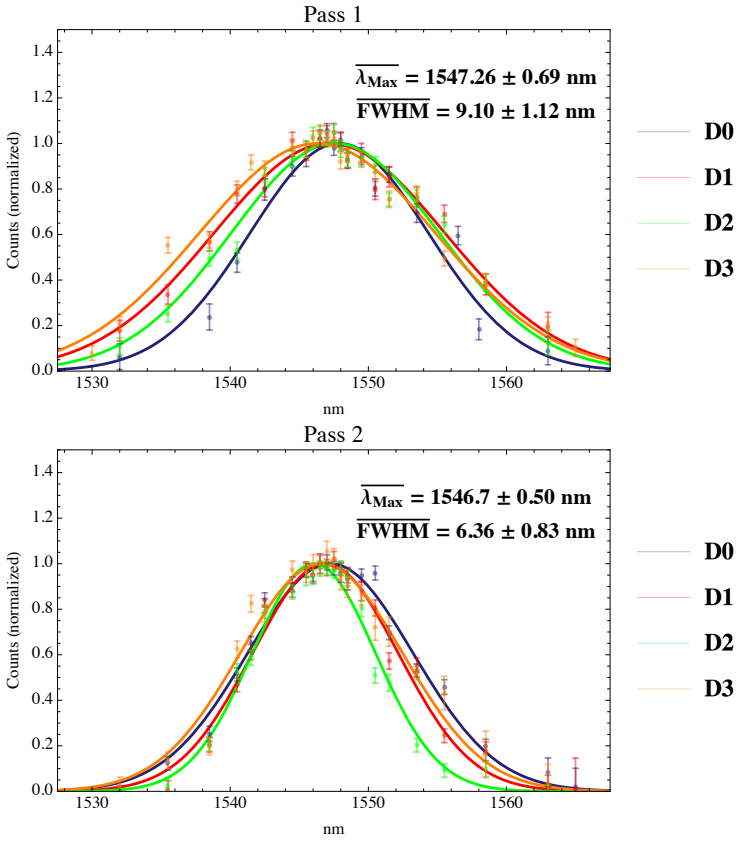

Figure S2: **Source spectral characterization.** Normalized spectral data from signal photons from both passes. D0 indicates Delay 0, and similarly for the other labels. $\bar{\lambda}_{max}$ is mean peak position and $\overline{\text{FWHM}}$ is mean full-width half maximum for all delays in a pass. Curves are best fits to a Gaussian.

III. ACCIDENTALS AND CAR PLOTS

A plot of accidental rates against reference power for the multiplexed and non-multiplexed sources is shown in Fig. S3a. A plot of coincidence rates against CAR, including data from the 4× multiplexed source and from Pass 2 is shown in Fig. S3b.

IV. THEORETICAL MODEL

A. Heralded single-photon source (HSPS) Model

We assume that strong spectral filtering on the idler arm and moderate filtering on the signal arm are sufficient such that the states produced by our sources are close to an idealized two-mode squeezed state with disentangled joint spectrums. Each source is characterized by three parameters: 1) an input power seed P_{seed} which relates the amount of input pump power to a reference photon generation probability from the crystal ($p_{pair} = 0.1$). 2) Idler transmission η_i, which is includes all sources of loss on the idler photon, such as from filters, coupling, and detector inefficiencies. The effect of nonlinear loss due to saturation effects from electronics and deadtime are treated in the next subsections. 3) Signal transmission η_s which is includes all sources of loss on the signal photon.

The relation between pump input power and effective squeezing parameter ξ for a down-conversion source is given by

$$\xi = \tanh\left(c\sqrt{P}\right), \tag{S3}$$

where P is the input power in units of mW and c is a coupling constant in units of $\text{mW}^{-1/2}$. The squeezing

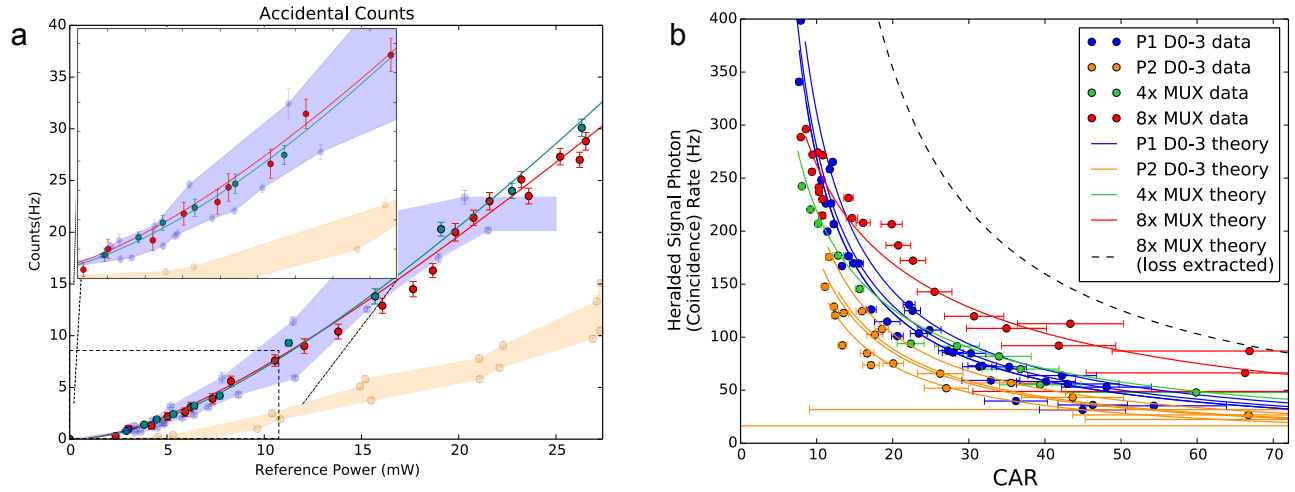

Figure S3: **Accidental and CAR plots. a,** Accidental rates vs. reference laser pump power for the 8x multiplexed (red), 4x multiplexed (blue), and non-multiplexed sources. For clarity, data points from the non-multiplexed sources are shown as linearly interpolated region plots encompassing the range of data: blue (Pass 1, Delays 0-3) and orange (Pass 2, Delays 0-3). P1 D0 indicates Pass 1, Delay 0, and similarly for the other labels. Theory lines for the multiplexed sources are calculated from measured heralded source parameters, measured switch loss, and extrinsic loss effects. Inset shows detail at low powers, where saturation effects due to electronics are small. **b, Heralded signal photon (coincidence) rate vs. CAR for multiplexed and non-multiplexed sources.** Red points are for the 8x multiplexed source, green points are for the 4x multiplexed source, blue points are for the non-multiplexed sources (Pass 1), and orange points are for the non-multiplexed sources (Pass 2). P1 D0 indicates Pass 1, Delay 0, and similarly for the other labels. Solid lines are based on a theory fit using measured parameters. Dashed line shows a correction for extrinsic sources of loss based on the theory model.

parameter ξ_{seed} corresponding to $p_{pair} = 0.1$ is $\xi_{seed} \approx .335715$, allowing for the extraction of the coupling constant c given a seed power P_{seed}. With this coupling constant, the squeezing parameters corresponding to any input power can be found.

Given a squeezing parameter ξ, idler transmission η_i , and signal transmission η_s, the probability for the idler (herald) arm to trigger using threshold detectors is given by [S19]:

$$p^i_{trig} = \frac{|\xi|^2 \eta_i}{1 - |\xi|^2 (1 - \eta_i)}. \tag{S4}$$

Given that the herald has triggered, the probability for a single-photon emission to lead to a detection event on the signal arm is

$$p^s_{single} = \left(1 - |\xi|^2\right) \eta_s \frac{\left[1 - \left(|\xi|^2 (1 - \eta_s)\right)^2 (1 - \eta_i)\right] \left[1 - |\xi|^2 (1 - \eta_i)\right]}{\left[1 - |\xi|^2 (1 - \eta_s)\right]^2 \left[1 - |\xi|^2 (1 - \eta_s)(1 - \eta_i)\right]^2}. \tag{S5}$$

Given that the herald has triggered, the probability for a multi-photon emission to lead to a detection event on the signal arm is

$$p^s_{multi} = \frac{Z_{TD}}{p^i_{trig}} - p^s_{single}, \tag{S6}$$

with

$$Z_{TD} = \left(1 - |\xi|^2\right) |\xi|^2 \left(\frac{1}{1 - |\xi|^2} + \frac{(1 - \eta_s)(1 - \eta_i)}{1 - |\xi|^2 (1 - \eta_s)(1 - \eta_i)} - \frac{(1 - \eta_i)}{1 - |\xi|^2 (1 - \eta_i)} - \frac{(1 - \eta_s)}{1 - |\xi|^2 (1 - \eta_s)} \right) \tag{S7}$$

Using these expressions we can find the probability of coincidence and accidental detection, and CAR (coincidence to accidental ratio).

B. Coincidences, accidentals, and CAR

We can find the probability of coincidence detection using threshold detectors, assuming the contribution from dark counts has been subtracted and pump leakage is negligible.

The probability of a coincidence is given by

$$Coin_{prob} = p^i_{trig}\left(p^s_{single} + p^s_{multi}\right). \tag{S8}$$

When seeded with a pump laser with repetition rate R, the expected coincidence rate is

$$Coin_{rate} = R \times Coin_{prob}. \tag{S9}$$

An accidental occurs when a coincidence between an idler and signal photon generated from two different pump pulses occurs, assuming the subtraction of dark counts and negligible pump leakage.

Without triggering from a herald, the signal photon trigger probability is given by

$$p^s_{trig} = \frac{|\xi|^2 \eta_s}{1 - |\xi|^2 (1 - \eta_s)}. \tag{S10}$$

Then a good approximation to the accidental probability is given by

$$Acc_{prob} = p^i_{trig} p^s_{trig}. \tag{S11}$$

The rate of accidental detection events is then

$$Acc_{rate} = R \times Acc_{prob}. \tag{S12}$$

The expected CAR, coincidence to accidental ratio, is then

$$CAR = Coin_{rate}/Acc_{rate}. \tag{S13}$$

C. Electronics saturation

In practice, saturation effects due to electronics and detector deadtimes will further affect the source performance. Assuming a detector has a deadtime of d, and that events are approximately uniformly distributed, the true rate of counts T from a detected rate of counts D can be approximated as [S32]

$$T = \frac{D}{1 - Dd}. \tag{S14}$$

Conversely, given an expected rate of counts T, the detected rate of counts will be

$$D = \frac{T}{dT + 1}. \tag{S15}$$

By applying these equations several times, the effect of several electronic deadtimes in series can be modeled. Most of the saturation effects in the experiment affect the idler arm, so these equations can be used to find an effective p^i_{trig} probability. Then, an effective η_i which includes loss due to saturation can be determined using equation S4.

Source	η_i	η_s	P_{seed} (mW)	$\overline{R^2}$
Pass 1 Delay 0	0.015	0.0019	5.2	0.993
Pass 1 Delay 1	0.015	0.0019	6.8	0.990
Pass 1 Delay 2	0.016	0.0021	5.6	0.988
Pass 1 Delay 3	0.017	0.0018	4.6	0.993

Table I: **Table showing source parameters for Pass 1.** Source parameters were determined using a numerical optimization fit to the model. $\overline{R^2}$ is the mean R^2 from the triggering rate, coincidence, and accidental fits.

D. HSPS Model fitting to data: Pass 1

Pass 1 has four time bins passing through the down-conversion crystal, which we will call Delay 0, Delay 1, Delay 2, and Delay 3. We will label these sources with the tuple $(pass, delay)$ corresponding to the pass and delay associated with the state source, for example Source $(1, 3)$ identifies the source from Pass 1 Delay 3.

Although in the ideal case each source would be exactly the same, in practice each source is slightly different: due to slight imperfections in alignment and optics, each source may feature different relative pump input powers, pump coupling, and different signal and idler loss rates.

Using the above model of the HSPS, a numerical optimization was performed to find the optimal input power seed P_{seed}, idler transmission value η_i, and signal transmission value η_s to match recorded value of heralding triggers, coincidences, and accidentals. We will label these parameters for each source with the corresponding tuple: $\eta_i^{(pass,delay)}$, $\eta_s^{(pass,delay)}$, $P_{seed}^{(pass,delay)}$. The model which maximized the mean R^2 statistic for APC counts, coincidences, and accidentals was found for all delays. These are shown in Table 1.

E. Time Multiplexed Source Model: Pass 1

The time multiplexed source is pumped by laser pulses which have been split into four pulses using free-space delay lines (Fig. S2), so the time multiplexed source model is constructed from the four HSPSs models from section D. Each HSPS in the time multiplexed source is pumped with a fraction of the total power used to pump the multiplexed source; the experimentally measured values were 0.2375, 0.2693, 0.2258, 0.2586 for Delay 0,1,2, and 3, respectively. The model for the time multiplexed source follows that of [S19], slightly modified to account for each time bin source being slightly different. In this section we neglect saturation effects; the same methods from section C can then be applied to the expected detection events to derive detection events with saturation.

The probability for the multiplexed source to trigger is given by

$$p_{trig}^{MUX,1} = 1 - \left(1 - p_{trig}^{i,(1,0)}\right)\left(1 - p_{trig}^{i,(1,1)}\right)\left(1 - p_{trig}^{i,(1,2)}\right)\left(1 - p_{trig}^{i,(1,3)}\right). \tag{S16}$$

When seeded with a pump laser with repetition rate R, the heralding rate is then

$$Trig_{rate}^{MUX,1} = R \times p_{trig}^{MUX,1}. \tag{S17}$$

Let $\eta_{sw}^{(pass,delay)}$ correspond to the transmission due to the switching network and variable delay lines for source $(pass, delay)$. Then the probability the heralded state is a single photon emission from source $(pass, delay)$, including the effect of the switching network with variable delay lines is $p_{single}^{s',(pass,delay)}$, given by replacing each instance of η_s in equation S5 with $\eta_s\eta_{sw}^{(pass,delay)}$. Similarly, the probability the heralded state is multi-photon emission from source $(pass, delay)$ is $p_{multi}^{s',(pass,delay)}$, is given by replacing each instance of η_s in equation S6 with $\eta_s\eta_{sw}^{(pass,delay)}$.

The coincidence probability is

$$Coin_{prob}^{MUX,1} = p_{trig}^{i,(1,0)} p_{single}^{s'(1,0)} + \left(1 - p_{trig}^{i,(1,0)}\right)\left(p_{trig}^{i,(1,1)} p_{single}^{s'(1,1)} + \left(1 - p_{trig}^{i,(1,1)}\right)\left(p_{trig}^{i,(1,2)} p_{single}^{s'(1,2)} + \left(1 - p_{trig}^{i,(1,2)}\right) p_{trig}^{i,(1,3)} p_{single}^{s'(1,3)}\right)\right). \tag{S18}$$

When seeded with a pump laser with repetition rate R, the expected coincidence rate is

$$Coin_{rate}^{MUX,1} = R \times Coin_{prob}^{MUX,1}. \tag{S19}$$

The accidental probability is

$$Acc_{prob}^{MUX,1} = p_{trig}^{i,(1,0)} p_{trig}^{s',(1,0)} + \left(1 - p_{trig}^{i,(1,0)}\right) p_{trig}^{i,(1,1)} p_{trig}^{s',(1,1)} + \left(1 - p_{trig}^{i,(1,0)}\right) \left(1 - p_{trig}^{i,(1,1)}\right) p_{trig}^{i,(1,2)} p_{trig}^{s',(1,2)}$$

$$\left(1 - p_{trig}^{i,(1,0)}\right) \left(1 - p_{trig}^{i,(1,1)}\right) \left(1 - p_{trig}^{i,(1,2)}\right) p_{trig}^{i,(1,3)} p_{trig}^{s',(1,3)}. \tag{S20}$$

The rate of accidental detection events is then

$$Acc_{rate}^{MUX,1} = R \times Acc_{prob}^{MUX,1}. \tag{S21}$$

The expected CAR, coincidence-to-accidental ratio, is then

$$CAR^{MUX,1} = Coin_{rate}^{MUX} / Acc_{rate}^{MUX}. \tag{S22}$$

Using measured values of switching loss and electronics saturation, the model was found to be in good agreement with the data (Main text: Fig. 3).

F. HSPS Model fitting to data: Pass 2

Pass 2 has two features different from Pass 1 (Section II). We used a simple model describing the effect of the back-reflected photon contamination. We assume the back-reflected photons on the signal arm are negligible. On the idler arm, we assume that every delay has the same probability of triggering due to a back-reflected photon as a fraction of the "true" triggering probability.

$$p_{trig\,back}^{i,(2,delay)} = p_{trig\,true}^{i,(2,delay)} \times f. \tag{S23}$$

Then the probability of "correctly" triggering is

$$p_{trig,correct}^{i,(2,delay)} = p_{trig\,true}^{i,(2,delay)} (1 - p_{trig\,back}^{i,(2,delay)}) + p_{trig\,true}^{i,(2,delay)} (p_{trig\,back}^{i,(2,delay)}), \tag{S24}$$

and the probability of "incorrectly" triggering is

$$p_{trig,incorrect}^{i,(2,delay)} = p_{trig\,back}^{i,(2,delay)} \left(1 - p_{trig\,true}^{i,(2,delay)}\right). \tag{S25}$$

Then the total probability for one arm to trigger is

$$p_{trig}^{i,(2,delay)} = p_{trig,correct}^{i,(2,delay)} + p_{trig,incorrect}^{i,(2,delay)}.$$

When seeded with a pump laser with repetition rate R, the heralding rate is then

$$Trig_{rate}^{i,(2,delay)} = R \times p_{trig}^{i,(2,delay)}. \tag{S26}$$

Following the techniques in [S19], we can derive the probability of single and multi photon detection given that the heralding detector has *not* triggered due to a paired idler photon:

$$p_{single\,no\,trig}^{i,(2,delay)} = \frac{\left(1 - |\xi|^2 (1 - \eta_i)\right) \eta_s (1 - \eta_i) |\xi|^2}{\left(1 - |\xi|^2 (1 - \eta_i)(1 - \eta_s)\right)^2}, \tag{S27}$$

Source	η_i	η_s	P_{seed} (mW)	$\overline{R^2}$
Pass 2 Delay 0	0.018	0.0024	6.3	0.971
Pass 2 Delay 1	0.017	0.0021	6.7	0.982
Pass 2 Delay 2	0.016	0.0023	6.8	0.978
Pass 2 Delay 3	0.015	0.0020	6.9	0.987

Table II: **Table showing source parameters for Pass 2.** Source parameters were determined using a numerical optimization fit to the model. $\overline{R^2}$ is the mean R^2 from the triggering rate, coincidence, and accidental fits.

$$p_{multi\,no\,trig}^{i,(2,delay)} = \left(1-|\xi|^2(1-\eta_i)\right)|\xi|^2\left(\frac{(1-\eta_i)}{1-|\xi|^2(1\text{-}\eta_i)} - \frac{(1-\eta_s)(1-\eta_i)}{1-|\xi|^2(1-\eta_s)(1-\eta_i)}\right) - p_{single\,no\,trig}^{i,(2,delay)}. \tag{S28}$$

Then the coincidence probability is

$$Coin_{prob}^{(2,delay)} = p_{trig,correct}^{i,(2,delay)}\left(p_{single}^{i,(2,delay)} + p_{multi}^{i,(2,delay)}\right) + p_{trig,incorrect}^{i,(2,delay)}\left(p_{single\,no\,trig}^{i,(2,delay)} + p_{multi\,no\,trig}^{i,(2,delay)}\right). \tag{S29}$$

The expected coincidence rate is

$$Coin_{rate}^{(2,delay)} = R \times Coin_{prob}^{(2,delay)}. \tag{S30}$$

The accidental probability is

$$Acc_{prob}^{(2,delay)} = p_{trig}^{i,(2,delay)} p_{trig}^{s,(2,delay)}. \tag{S31}$$

and the expected accidental rate is

$$Acc_{rate}^{(2,delay)} = R \times Acc_{prob}^{(2,delay)}.$$

The model which maximized the mean R^2 statistic for APC counts, coincidences, and accidentals was found for all delays. These are shown in Table 2.

G. Time Multiplexed Source Model: Pass 2

The probability for the MUX source from Pass 2 to trigger is

$$p_{trig}^{MUX,2} = 1-(1-p_{trig}^{i,(2,0)})(1-p_{trig}^{i,(2,1)})(1-p_{trig}^{i,(2,2)})(1-p_{trig}^{i,(2,3)}), \tag{S32}$$

and the expected heralding rate is

$$Trig_{rate}^{MUX,2} = R \times p_{trig}^{MUX,2}. \tag{S33}$$

The coincidence probability is

$$Coin_{prob}^{MUX,2} = Coin_{prob}^{(2,0)'} + \left(1-p_{trig}^{i,(2,0)}\right)\left(Coin_{prob}^{(2,1)'} + \left(1-p_{trig}^{i,(2,1)}\right)\left(Coin_{prob}^{(2,2)'} + \left(1-p_{trig}^{i,(2,2)}\right)Coin_{prob}^{(2,3)'}\right)\right). \tag{S34}$$

where $Coin_{prob}^{(2,delay)'}$ is given by $Coin_{prob}^{(2,delay)}$ except with every instance of η_s replaced with $\eta_s\eta_{sw}^{(2,delay)}$.
The expected coincidence rate is

$$Coin_{rate}^{MUX,2} = R \times Coin_{prob}^{MUX,2}. \tag{S35}$$

The accidental probability is

$$Acc_{prob}^{MUX,2} = p_{trig}^{i,(2,0)} p_{trig}^{s',(2,0)} + \left(1 - p_{trig}^{i,(2,0)}\right) \left(p_{trig}^{i,(2,1)} p_{trig}^{s',(2,1)} + \left(1 - p_{trig}^{i,(2,1)}\right) \left(p_{trig}^{i,(2,1)} p_{trig}^{s',(2,1)} + \left(1 - p_{trig}^{i,(2,2)}\right) p_{trig}^{i,(2,0)} p_{trig}^{s',(2,1)}\right)\right), \tag{S36}$$

where $p_{trig}^{s',(2,delay)}$ is given by $p_{trig}^{s,(2,delay)}$ except with every instance of η_s replaced with $\eta_s \eta_{sw}^{(2,delay)}$.
The expected accidental rate is

$$Acc_{rate}^{MUX,2} = R \times Acc_{prob}^{MUX,2}. \tag{S37}$$

H. Time and Space Multiplexed Source Model: Both Passes

The probability for the complete multiplexed source to trigger is

$$p_{trig}^{MUX} = 1 - \left(1 - p_{trig}^{MUX,1}\right) \left(1 - p_{trig}^{MUX,2}\right), \tag{S38}$$

and the expected heralding rate is

$$Trig_{rate}^{MUX} = R \times p_{trig}^{MUX}. \tag{S39}$$

The coincidence probability is

$$Coin_{prob}^{MUX} = Coin_{prob}^{MUX,1} + \left(1 - p_{trig}^{MUX,1}\right) Coin_{prob}^{MUX,2}. \tag{S40}$$

The expected coincidence rate is

$$Coin_{rate}^{MUX} = R \times Coin_{prob}^{MUX}. \tag{S41}$$

The accidental probability is

$$Acc_{prob}^{MUX} = Acc_{prob}^{MUX,1} + \left(1 - p_{trig}^{MUX,1}\right) Acc_{prob}^{MUX,2}. \tag{S42}$$

The expected accidental rate is

$$Acc_{rate}^{MUX} = R \times Acc_{prob}^{MUX}. \tag{S43}$$

The expected CAR is

$$CAR^{MUX} = Coin_{prob}^{MUX} / Acc_{prob}^{MUX}. \tag{S44}$$

Using measured values of switching loss and electronics saturation, the model was found to be in good agreement with the data (Main Text: Fig. 4).

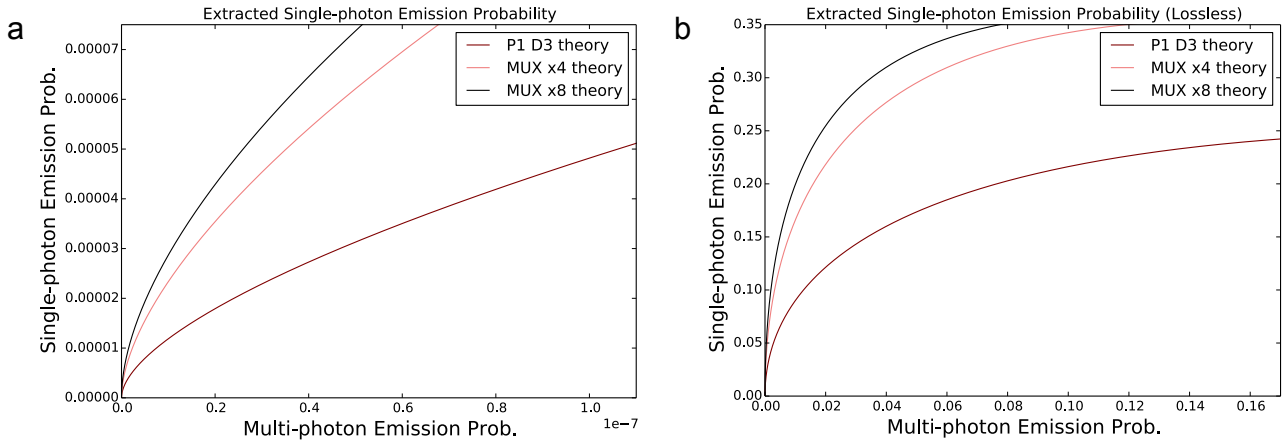

Figure S4: **Extracted theoretical single-photon emission probability for multiplexed and non-multiplexed sources. a,** Model with extrinsic sources of loss removed. **b,** Model with all sources of loss except switch loss and power loss removed.

V. SINGLE-PHOTON EMISSION ENHANCEMENT

Using the model with extrinsic sources of loss removed, we can extract the heralded single-photon emission probabilities for fixed multi-photon emission probabilities of the 8× and 4× multiplexed sources and the best performing non-multiplexed source (Fig. S4a). We include the loss of final measurement detector.

To further examine the long-term prospects of the multiplexed source, we can also remove all sources of loss, except those due to the multiplexing switches and power loss affecting the second pass. These sources of loss include filtering, coupling, and detector inefficiencies (although we still assume the use of threshold detectors). The extracted single-photon emission probabilities for fixed multi-photon emission probabilities of the 8× and 4× multiplexed sources and the best non-multiplexed source are shown in Fig. S4b. The multiplexed sources tend towards the theoretical limit (50%) achievable using threshold detectors (number-resolving detectors enable a single-photon emission probability tending towards 1).